Multi-functional hindered amine light stabilizers-functionalized carbon nanotubes for advanced ultra-high molecular weight Polyethylene-based nanocomposites

N.Tz. Dintcheva [a,*], R. Arrigo [a], E. Morici [a], C. Gambarotti [b], S. Carroccio [c], F. Cicogna [d], G. Filippone [e]

[a] *Dipartimento di Ingegneria Civile, Ambientale, Aerospaziale, dei Materiali, Università di Palermo, Viale delle Scienze, Ed. 6, 90128 Palermo, Italy*
[b] *Department of Chemistry, Materials and Chemical Engineering "Giulio Natta", Politecnico di Milano, Piazza Leonardo da Vinci, 32, 20133 Milano, Italy*
[c] *CNR-IPCB-Section of Catania, Via P. Gaifami, 18, 95126 Catania, Italy*
[d] *Istituto di Chimica dei Composti Organo Metallici (ICCOM), Consiglio Nazionale delle Ricerche, UOS Pisa, Via G. Moruzzi 1, 56124 Pisa, Italy*
[e] *Dipartimento di Ingegneria Chimica, dei Materiali e della Produzione Industriale, Università di Napoli Federico II, Piazzale V. Tecchio, 80, 80125 Napoli, Italy*

Received 30 January 2015
Received in revised form
11 May 2015
Accepted 30 July 2015
Available online 6 August 2015

1. Introduction

The development of innovative multi-functional hybrid carbon-based nanoparticles and their polymer nanocomposites have gained a great interest among researchers in the last two decades [1–3]. One of the most promising candidates for the design of novel multi-functional nanoparticles are carbon nanotubes [4,5] whose high aspect ratio and carbonaceous nature provide them with unique properties, such as high electrical and thermal conductivity, electro-optical behaviour, chemical reactivity, and excellent mechanical stiffness. The superior properties of CNTs make them attractive for the formulation of advanced and high performance polymer-based composites, suitable for applications in such different areas ranging from biomedical engineering, optical electronics, ultra filtration, energy storage, and photovoltaic cells [6,7]. Nevertheless, the performance of CNTs/polymer nanocomposites depends on the dispersion of CNTs in the host matrix and on the established interfacial interactions. Therefore, significant efforts have been directed towards developing methods to modify surface properties of CNTs and to improve their compatibility with host polymer matrices. The chemical functionalization of CNTs, that can be achieved through different methods, such as covalent linkage [6], non-covalent supramolecular absorption [7], defect functionalization [8] or modification through click chemistry [9]. Besides improving their dispersibility inside polymer matrices [10–12], such chemical modifications provides the CNTs with new functionalities, thus enlarging their possible fields of application [13,14]. In particular, CNTs can be profitably used as nano-carriers bearing specific functionalities to be dispersed in a polymer matrices. This strategy, which combines all the structural advantages of this 1D nanofiller with the specific properties of the functional groups, allows to obtain innovative multi-functional

* Corresponding author. Tel.: +39 091 23863704; fax: +39 091 23860841.
E-*mail address:* nadka.dintcheva@unipa.it (N.Tz. Dintcheva).

nanoparticles with several potential applications. In our previous works, CNTs bearing natural natural stabilizing molecules, such as vitamin E and quercetin, revealed to be able to greatly enhance the thermo-oxidative resistance of a host polymer [15–17]. The results have been explained considering that the natural anti-oxidant molecules boost up the intrinsic radical scavenging activity of CNTs [18,19]. The latter can be further increased through the insertion of specific anti-oxidant functionalities [20] or UV-stabilizers [21] on the outer surface of CNTs. Indeed, a recent study by Lonkar et al. [21] evidenced that MWCNTs modified with Hindered Amine Light Stabilizer (HAS) dispersed in polypropylene (PP) matrix are able both to increase the induction period of PP photo-oxidation and to improve the mechanical properties of the nanocomposites. HAS molecules are well-known to provide poly-olefins with long-term stability through a well-documented mechanism that involves the formation of nitroxyl (NO) radicals. The latter are able to scavenge alkyl radicals formed during poly-mers oxidation. The HAS efficiency is due to the fact that, in the course of these reactions, NO radicals are regenerated according to the "Denisov cycle" [22].

In the specific case of Ultra High Molecular Weight Polyethylene (UHMWPE), and particularly in the radiation cross-linked material used in the design of artificial joints, HAS molecules have been suggested as possible stabilizers in place of the currently used Vitamin E (VE) [23]. HAS were proved to have better performances than VE due to the different stabilization mechanisms of the two classes of stabilizers. In particular, a fraction of VE can react with alkyl radicals already during the step of radiation cross-linking of UHMWPE. On the one hand, this leads to a reduction of radiation efficiency or cross-link density; on the other hand, part of VE becomes no longer available for the protection of the cross-linked polymer during their useful lifetime. In contrast, being added in a non radical form, HAS do not interfere with the cross-linking mechanism. Only after irradiation and in the presence of oxygenated species HAS are activated, giving rise to nitroxides able to react with radical species so as to stabilize the host polymer.

Currently UHMWPE components are limited in their thickness due to concerns about elevated stresses and the potential for fracture. Therefore, there is increased interest in UHMWPE composites to improve the strength of the material, without sacrificing its excellent performance such as bio-compatibility and wear resistance [24–26].

In this work, HAS molecules have been anchored on the outer surface of CNTs, and the obtained multi-functional fillers (HAS-*f*-CNTs) have been used for the formulation of advanced Ultra High Molecular Weight Polyethylene (UHMWPE) nanocomposites. The UHMWPE/HAS-*f*-CNTs nanocomposite exhibits segregated morphology consisting of conductive nanoparticles paths spanning the host matrix. More importantly, the HAS-*f*-CNTs provide high photo-oxidative stability due to a synergic effect of HAS and CNTs, which are not as effective if used separately.

2. Experimental part

2.1. Materials

The UHMWPE is a commercial grade purchased by Sigma–Aldrich in the form of a white powder. Its main properties are: average molecular weight M_w = 3÷6 MDa, softening point T = 136 °C (Vicat, ASTM D 1525B), melting point T_m = 138 °C and density ρ = 0.94 g/mL at 25 °C.

CNTs bearing hindered amine light stabilizer molecules (HAS) grafted on the outer surface (HAS-*f*-CNTs) were produced starting from multiwalled CNTs containing ~1 wt.% of covalently linked –COOH groups (CNTs-COOH) purchased by Cheap Tubes, U.S.A. Their main features are: outer diameter OD = 120÷180 nm, inner diameter ID = 10÷20 nm, length L = 10÷20 μm, purity >95 wt.%, ash <1.5 wt.%, specific surface area SSA>60 m^2/g and electrical conductivity $EC > 10^{-2}$ S/cm. Bare multiwalled CNTs were used to produce reference samples. They have OD = 120÷180 nm, ID = 10÷20 nm, L = 10÷20 μm, purity >95 wt.%, ash <1.5 wt.%, SSA>40 m^2/g and $EC > 10^{-2}$ S/cm.

N,N'-dicyclohexylcarbodiimide (DCC) and 2,2,6,6-tetramethyl-4-piperidinol (light stabilizer molecules, HAS) were purchased from Sigma–Aldrich and utilized without further purifications.

4-piperidol,2,2,6,6-tetramethyl-RPW stearin, a commercial light stabilizer with trade name Cyasorb® UV-3853 (UV-3853), was supplied by Cytec.

2.2. Side-wall functionalized CNTs-COOH

The covalent linkage between the side-wall carboxylic function of the CNTs (1) and the piperidinol (3) was obtained by esterification in the presence of DCC (see Fig. 1). Due to steric hindrances, the endocyclic amino function of 2,2,6,6-tetramethyl-4-piperidinol is rather inert in the reaction conditions, and only the hydroxyl group is involved in the esterification.

0.2 g of CNTs (1) were dispersed in a solution of 2,2,6,6-tetramethyl-4-piperidinol (3) (0.64 mmol, 0.10 g) and DCC (0.19 mmol, 0.040 g) in 30 mL of dry THF. The resulting mixture was sonicated in an ultrasound bath (240 W, 2.5 Lt) for 1 min then stirred at ambient temperature under nitrogen atmosphere for 96 h. After that time, the suspension was filtered using a sintered glass filter. Afterward, the CNTs were washed with hot N,N'-dimethylformamide and methanol under vigorous stirring, repeating the procedure up to 10 times before drying at 90 °C overnight.

2.3. Nanocomposite preparation

UHMWPE-based nanocomposites containing 1 wt.% of bare CNTs, CNTs-COOH or HAS-*f*-CNTs were prepared by hot compaction (HC) using a hydraulic Carver press. Polymer and CNTs were manually mixed at room temperature to obtain a homogeneous black powder, which was loaded between the plates of the press and compressed at a pressure P = 1500 psi for 5 min at temperature T = 210 °C. The resulting thin films (thickness ~80 μm) were used for the subsequent analyses. HC films based on pure UHMWPE and UHMWPE/UV-3853 containing 0.5 wt.% of free stabilizer were used as reference samples.

2.4. Characterization

Attenuated Total Reflectance – Fourier Transform Infrared Spectroscopy (ATR-FTIR) analysis of CNTs-COOH and HAS-*f*-CNTs was performed using a Spectrum Two FTIR spectrometer (Perkin Elmer) equipped with a diamond crystal for surface analysis. ATR-FTIR spectra collected on three different batches of each sample (milligram level) were obtained by accumulation of 32 scans between 4000 and 1000 cm^{-1}, with a resolution of 4 cm^{-1}.

Thermogravimetric analyses (TGA) were carried out on the bare and functionalized CNTs by using an Exstar TG/DTA Seiko 7200 instrument. The tests were performed at a heating rate of 10 °C/min from 30 to 750 °C under nitrogen flow. The reported results are the average of three independent measurements on batches of ~5 mg. The standard deviation was ±0.3% for each investigated sample.

Micro-Raman spectroscopy has been performed at room temperature through a Bruker-Senterra micro-Raman equipped with a 532 nm diode laser excitation and 20 mW power. Non-confocal

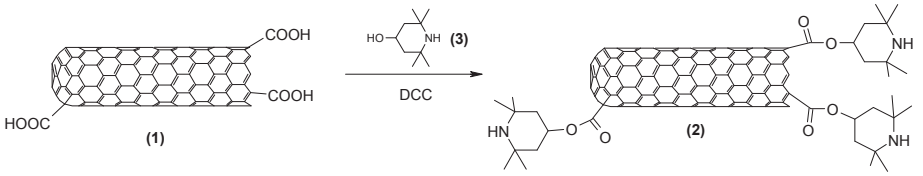

Fig. 1. Scheme of side-wall functionalization of CNTs by 2,2,6,6-tetramethyl-4-piperidinol.

measurements were carried out in the range 4000–400 cm^{-1} with a spectral resolution between 9 and 15 cm^{-1}.

Pyrolysis Gas Chromatography Mass Spectrometry (Py-GCMS) experiments were carried out on a Frontier Laboratories' Multi-Shot Pyrolyzer EGA/PY-3030D with direct connection to a Shimadzu GCMS-TQ8040 gas chromatography mass spectrometer (GC-MS) equipped with a 30 m × 0.25 mm inner diameter (5%-phenyl)-methylpolysiloxanenon-polar column (HP5MS). The pyrolyzer was set at 350 °C and kept at this temperature till the end of experiment. The GC/MS conditions were the following: inlet temperature at 250 °C, pressure 7.1 psi, split ratio 50:1. The oven temperature of the GC was held at 40 °C for 1 min followed by continuous heating (6 °C/min) to 280 °C with 1 mL/min helium carrier gas. Then, the final temperature was held for 15 min to ensure that no heavy molecules remained in the column. The mass spectrometer conditions used were: transfer line temperature 150 °C, ion source temperature 230 °C, and electron impact ionization (EI) at 70 eV.

Rheological tests were performed using a strain-controlled rheometer (mod. ARES G2 by TA Instrument) in parallel plate geometry (plate diameter 25 mm). The complex viscosity (η^*) was measured performing frequency scans from $\omega = 10^{-1}$ to 10^2 rad/s at $T = 210$ °C. The strain amplitude was $\gamma = 2\%$, which preliminary strain sweep experiments proved to be low enough to be in the linear viscoelastic regime.

Optical microscopy was performed using a Leica Microscope in reflection mode at a magnification of 20×. Images were acquired on the surface of the nanocomposite films.

Transmission Electron Microscopy (TEM) observations were performed at the Centro Grandi Apparecchiature – UninetLab, University of Palermo. The analyses were carried out on ultrathin films with thickness of about 100 nm, prepared via cutting from specimens block with a Leica Ultramicrotome EMUC6. The ultrathin slides were mounted on lacey carbon films on 300 mesh copper grids and then observed using a Jeol JEM-2100 at 200 kV.

Scanning Electron Microscopy (SEM) observation were performed using a Phenom ProX desktop SEM on the surface of ultrathin films, prepared via cutting from specimens block with a Leica Ultramicrotome EMUC6.

Electrical resistivity of each film was measured employing a commercial setup (ECOPIA HMS-3000, B = 0.55 T) at room temperature.

Dynamic Mechanical Thermal Analysis (DMTA) was performed using a Rheometrics DMTA V instrument, single cantilever bending method. The test has been carried out in the temperature swift mode, between 10 and 120 °C at a heating rate of 2 °C/min. The frequency was set to 1 Hz and the maximum strain amplitude was 0.5%. The elastic modulus (E′) as a function of the temperature was recorded.

Photo-oxidation of polymer films, about 100 μm thick, was carried out using a Q-UV-Solar Eye weatherometer (from Q-LAB, USA) equipped with UVB lamps (313 nm). The weathering conditions were 8 h of light at T = 55 °C followed by 4 h of dark/condensation at T = 35 °C. The progress of the photo-degradation was followed analysing the evolution in time of FTIR spectra on polymer films (thickness about 100 μm) carried out by using a Perkin Elmer FT-IR spectrometer (mod. Spectrum Two). FTIR spectra collected on three different films of each sample were obtained by performing 16 scans between 4000 and 500 cm^{-1}. The photo-oxidation evolution was quantified by referring to the carbonyl (CI) and hydroxyl (HI) indices as a function of irradiation time. CI was calculated as the ratio between the integral of the carbonyl absorption region (1850–1600 cm^{-1}) and that of a reference peak at about 1370 cm^{-1}; HI refers to the hydroxyl absorption region (3570–3150 cm^{-1}), which integral was normalized by the peak at 1370 cm^{-1}.

All the experiments were carried out at least in duplicate to verify the robustness of the results.

3. Results and discussion

3.1. Characterization of HAS-f-CNTs

Reactive hindered amine light stabilizer molecules were grafted onto the outer surface of the CNTs-COOH (see Fig. 1), and the surface functionalization was assessed through ATR-FTIR, Raman spectroscopy, TGA and mass spectrometry. The ATR-FTIR spectra of CNTs-COOH and HAS-*f*-CNTs are shown in Fig. 2. The spectrum of the HAS-*f*-CNTs displays a strong absorption band at 2966 cm^{-1} and a broad absorption band centred at around 2852 cm^{-1} due to the asymmetrical ($\nu_{as}CH_3$) and symmetrical (ν_sCH_3) stretching of C–H bonds in methyl groups, respectively. Besides, a broad absorption band centred at around 3100 cm^{-1} possibly due to N–H stretching vibration of the grafted functional group is also visible [27]. Unfortunately, due to the strong absorbance feature of CNTs,

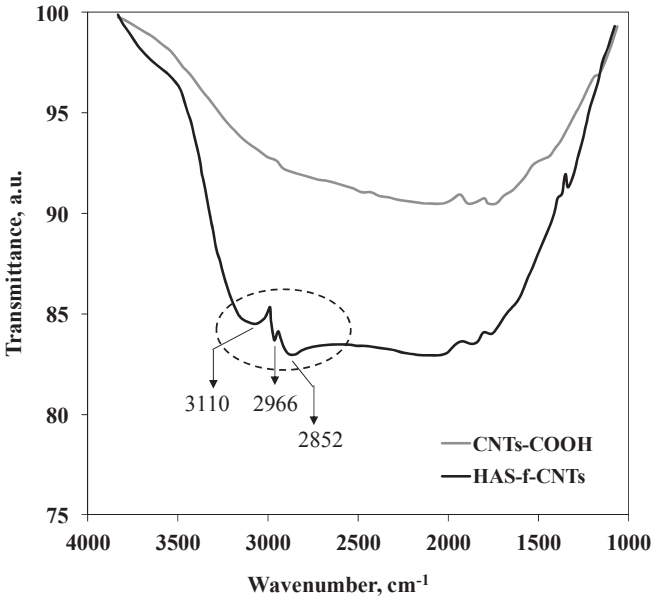

Fig. 2. ATR-FTIR spectra of CNTs-COOH and HAS-*f*-CNTs.

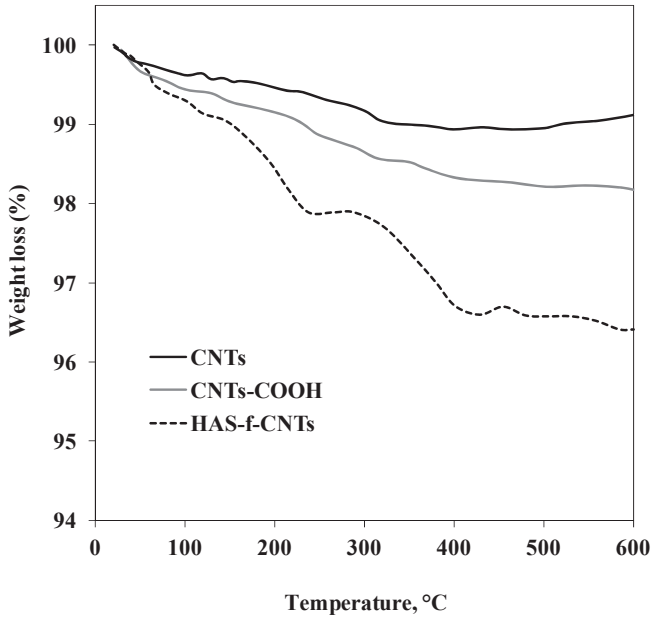

Fig. 3. TGA curves of bare CNTs, CNTs-COOH and HAS-*f*-CNTs.

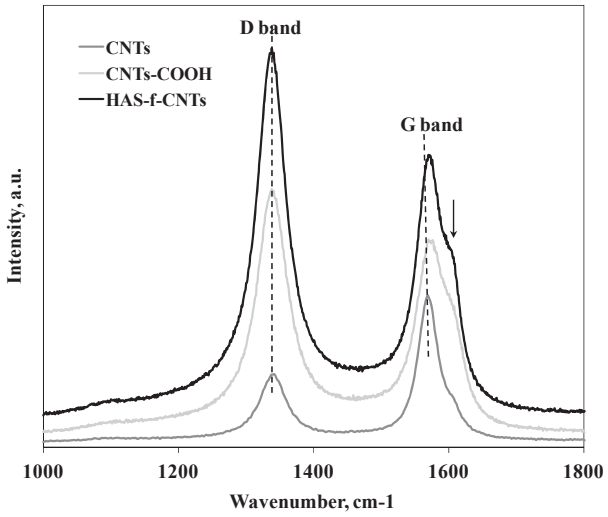

Fig. 5. Raman spectra of bare CNTs, CNTs-COOH and HAS-*f*-CNTs.

the ATR-FTIR analysis is not conclusive about the chemical immobilization of HAS molecules, since the functional groups are hardly visible. More convincing proofs about occurred HAS grafting come from TGA analysis. Both the CNTs-COOH and HAS-*f*-CNTs decompose faster than the bare CNTs with increasing the temperature. This is a consequence of the volatilization of the grafted carboxyl and HAS molecules. The gradual weight loss related to the thermal decomposition of the HAS groups takes place in the range 300÷400 °C, i.e. well above the temperature at which the nanocomposite thin films were prepared and characterized. Probably, the weight loss up to 100 °C is due to a small amount of residual water in all the samples. The residues at the end of the analysis were 98.1 wt.% and 96.5 wt.% for CNTs-COOH and HAS-*f*-CNTs, respectively, whereas a residual of 99.1 wt.% was found for the bare CNTs due to a partial decomposition of the bulk material, see Fig. 3. Therefore, the overall content of HAS from the gradual mass loss of HAS-*f*-CNTs was estimated to be around 2.0 wt.% (see Fig. 3).

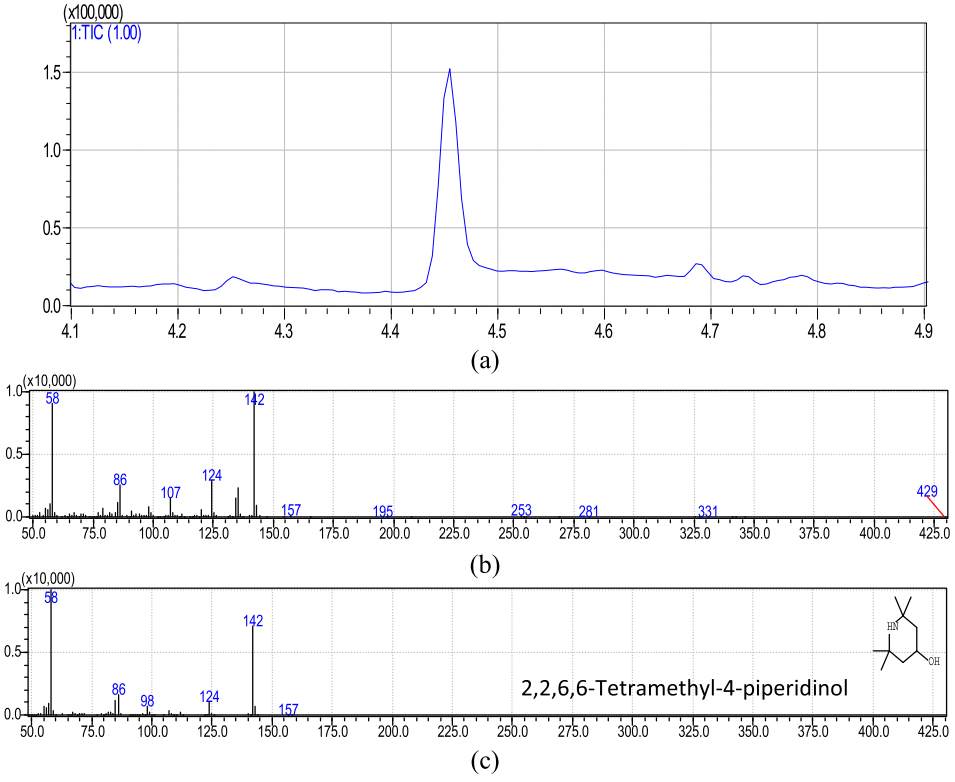

Fig. 4. (a) An enlargement portion of Py-GC signal assigned to 2,2,6,6-tetramethyl-4-piperidinol in Py-GC MS and (b) corresponding mass spectrum matched with (c) database mass spectrum of 2,2,6,6-tetramethyl-4-piperidinol.

The surface functionalization of CNTs with HAS was further confirmed by the GC-MS analysis of the pyrolyzed HAS-*f*-CNT. An enlargement portion of GC signal assigned to 2,2,6,6-tetramethyl-4-piperidinol in Py-GC MS is shown in Fig. 4, together with the corresponding mass spectrum of 2,2,6,6-tetramethyl-4-piperidinol. The almost total matching between the MS spectra of our sample (spectrum b) and database mass spectra (spectrum c) can be observed, which confirms the presence of 2,2,6,6-tetramethyl-4-piperidinol.

According to our previous study [15], CNTs lattice defect due to the functionalization can be detected by the Raman spectroscopy by considering the ratio between the signal intensities of the disorder-induced D-band at ~1340 cm^{-1} (I_D) and tangential G-band at ~1570 cm^{-1} (I_G) [28,29]. The Raman spectra of bare CNTs, CNTs-COOH and HAS-*f*-CNTs sample are compared in Fig. 5.

The I_D/I_G ratio of bare CNTs is about 0.47, while it increases significantly for both CNTs-COOH ($I_D/I_G = 1.12$) and HAS-*f*-CNTs ($I_D/I_G = 1.40$) samples. This indicates that the presence of carboxylic groups and, even more, of HAS molecules, allows for the formation of a large amount of surface defects. Furthermore, a slight shift of tangential G-band for HAS-*f*-CNTs compared to the bare CNTs and intensification of the shoulder centred at around 1605 cm^{-1} are due to the modification occurring in the structure of CNTs, which further confirms the successful grafting of HAS [29].

3.2. Characterization of UHMWPE-based nanocomposites

The molecular architecture changes in polymers and polymer-based nanocomposites may be gainfully investigated through rheology analysis. Additionally, the rheological analysis of nano-filled polymers provides valuable information in terms of state of dispersion of the nanoparticles. The complex viscosity curves (η^*) and elastic (G') and loss (G'') moduli of neat UHMWPE and investigated nanocomposites as a function of frequency are shown in Fig. 6(a and b). The addition of free HAS molecules (UV-3853) causes a slight reduction of the rheological functions with respect to neat UHMWPE likely due to a plasticizing effect exerted by the low molecular weight additive. Concerning the effect of the nanotubes addition, the η^* values of all nanocomposites are slightly higher than those of neat UHMWPE in the whole investigated frequency range. Bare and COOH-functionalized CNTs have an irrelevant effect, resulting in a mere vertical shift of the η^* curve, without actually altering the relaxation spectrum of matrix macromolecules. This feature is typical of not uniformly dispersed fillers. Differently, the HAS-*f*-CNTs are able to generate appreciable rheological alterations. In particular, the upturn of η^* at the lowest investigated frequency could is indicative of interconnected superstructures that span portions of the host matrix. Alterations in the low frequency behaviour emerge also in the elastic shear modulus G', which increases upon addition of CNTs. Again, the effect is more prominent in case of HAS-F-CNTs.

The morphological inspections of the nanocomposite films confirm the presence of continuous paths of CNTs throughout the matrix guessed from the rheological analysis. Representative optical, SEM and TEM micrographs of the UHMWPE-based nanocomposites containing bare CNTs, CNTs-COOH and HAS-*f*-CNTs are shown in Fig. 7. The CNTs appear as the dark phase. A segregated microstructure is noticed, in which the CNTs are mainly localized in the interfacial regions between UHMWPE particles. This is a direct consequence of the selected compounding method: the CNTs cover the surface of the polymer particles in the initial UHMWPE/nanoparticles mixture, remaining at the boundaries between the polymer particles at the end of the process. As a result, the formation of CNTs-rich channels around UHMWPE-rich islands is achieved [24]. The SEM observations provide further evidence of the segregated morphology. Some differences appears between the samples containing bare and functionalized CNTs. The former are arranged in a broader segregated networks within host matrix, which is probably due to some re-aggregation phenomena between CNTs that hinder their distribution in the interfacial regions. Better segregated structures are instead noticed in the presence of COOH- and HAS-*f*-CNTs. The functional groups could favour the CNT distribution, eventually promoting the formation of better segregated microstructure. TEM analyses reveal that the CNTs are in the form of tangled bundles. The effects of CNT functionalization are difficult to be appreciated over the short length scale of TEM investigations.

These observed segregated networks are beneficial to form conductive nanoparticles paths through the host matrix. The electrical resistivity of neat UHMWPE and CNTs containing nanocomposites is reported in Table 1. As expected, the unfilled UHMWPE shows highest values of resistivity. The addition of bare CNTs causes a drop of two orders of magnitude of the resistivity, which further decreases when CNTs-COOH and HAS-*f*-CNTs are used. This corroborates the hypothesis of a beneficial effect of the presence of functional groups on the outer surface of the CNTS in terms of nanotube dispersion and formation of segregated morphology. It is interesting to highlight that the presence of HAS moiety on the CNT outer surface does not affect negatively the

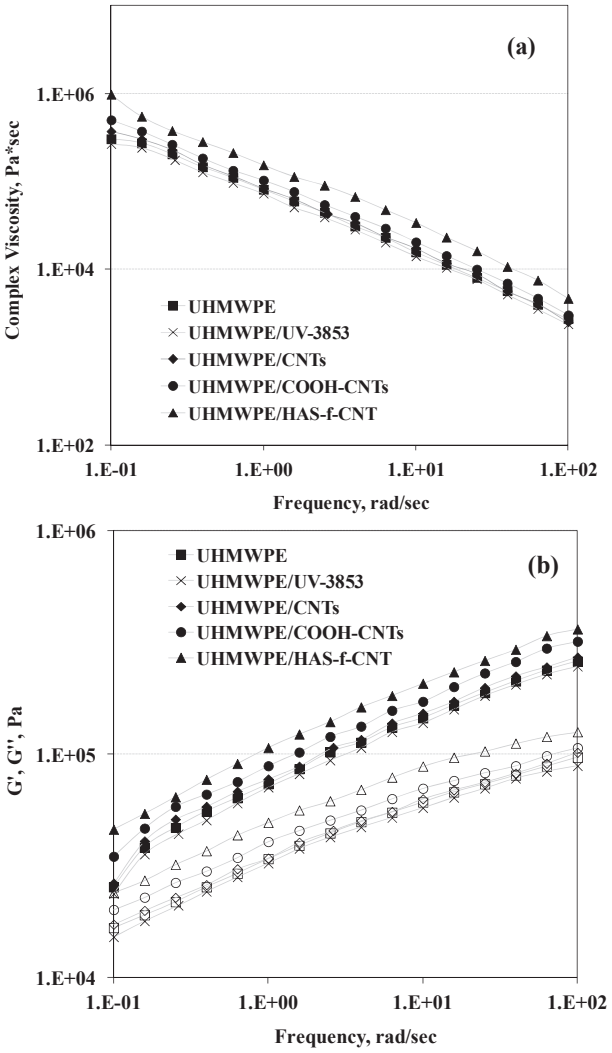

Fig. 6. (a) Complex viscosity curves (η^*) and (b) elastic (G') and loss (G'') moduli of neat UHMWPE and investigated nanocomposites.

formation of the conductive channels around UHMWPE-rich islands. This suggests the possibility to use HAS-*f*-CNTs as multifunctional fillers for the formulation of advanced innovative polymer-based nanocomposites.

To investigate the mechanical behaviour of the nanocomposites, the elastic modulus (E′) collected through DMA analyses is reported in Fig. 8 as a function of the temperature for neat UHMWPE and all nanocomposites. The presence of free UV-3853 molecules has a negligible effect on the elastic modulus. The CNTs-containing samples show less pronounced temperature dependence and higher E′ values than neat UHMWPE. In line with rheological analyses, such a reinforcing effect is more pronounced for the HAS-f-CNTs, which double the modulus at room temperature and triplicate it at 100 °C (see inset of Fig. 8). The obtained segregate morphology of the CNTs-containing samples could be considered responsible for the enhanced mechanical behaviour.

3.3. Photo-oxidation behaviour of UHMWPE-based nanocomposites

To investigate the photo-oxidation behaviour of UHMWPE-based nanocomposites, thin films have been subjected to accelerate UVB exposure and the formation of carbonyl and hydroxyl species as a function of the exposure time has been monitored through FTIR analysis. The calculated carbonyl (CI) and hydroxyl (HI) indices of investigated systems are shown in Fig. 9. The CI refers to the signals in the range 1850 to 1600 cm^{-1}, which are due to the formation of different amount of carbonyl species and reflect the formation of acid (1715 cm^{-1}), ketones (1718 cm^{-1}), esters (1738 cm^{-1}) and lactones (1786 cm^{-1}). The HI is related to the presence of linked and free −OH groups deriving from the photo-oxidation process. In order to facilitate the comparison between the samples, we introduce a kind of induction time for the oxidation processes, t_i, which is conventionally defined as the time needed for CI reaches the value of 5 and HI reaches 2: for times $t < t_i$ the indices grow very slowly, while around t_i a sudden switch of the kinetics takes place, and the growth becomes very fast reflecting the progress of degradation. The estimated t_i values are summarized in Table 2. The quantitative agreement between the values computed from CI and HI indicates that both indices are suited for monitoring the degradation of UHMWPE.

The neat UHMWPE does not experience significant oxidative processes until about 300 h of UVB exposure; afterwards, oxidation suddenly begins due to the rapid formation of oxidized species such as acids, ketones and esters. It is important to observe that such chemical reactions are generally coupled with a noticeable worsening of the mechanical properties.

As expected, the addition of free non-volatile UV-3853 molecules delays the oxidation induction time due to the well known protective action of the hindered amines against photo-oxidation.

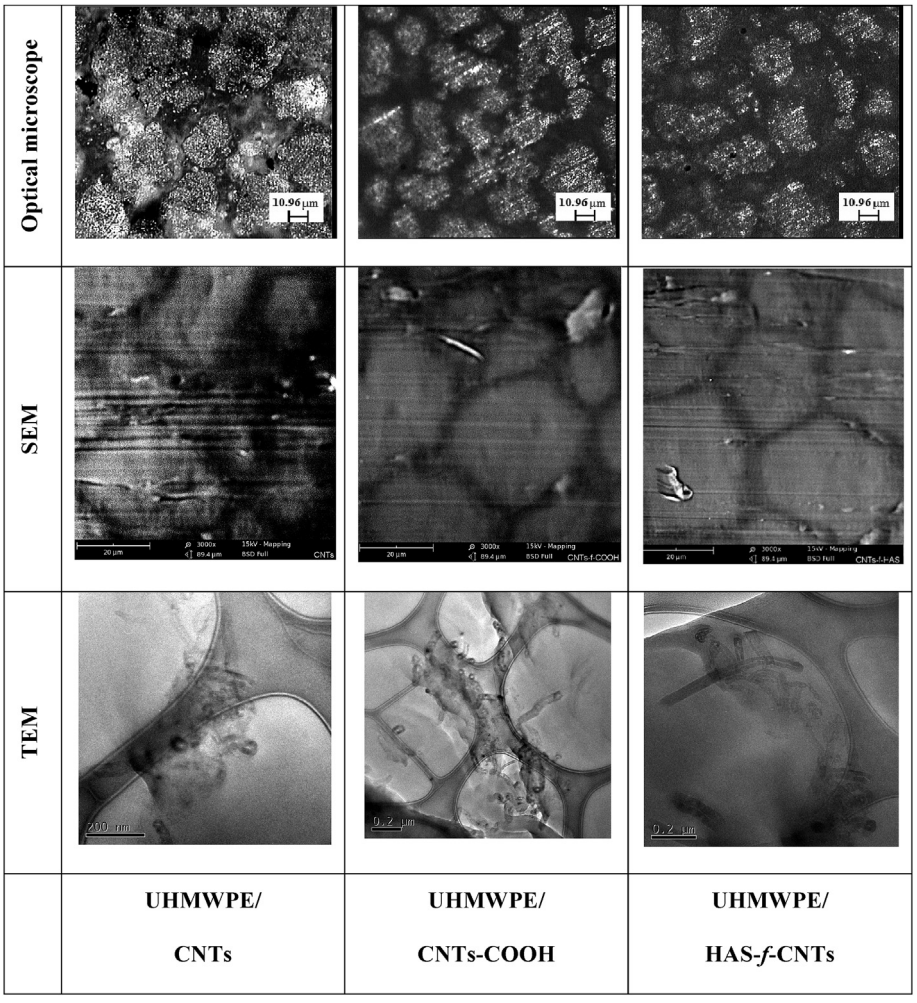

Fig. 7. Morphological observations at different length scales of all investigated UlHMWPE-based nanocomposites.

Table 1
Electrical resistivity values for neat UHMWPE and all investigated nanocomposites.

	ρ [Ω*m]
UHMWPE	$1.1*10^8$
UHMWPE/CNTs	$1.6*10^6$
UHMWPE/COOH-CNTs	$7.7*10^5$
UHMWPE/HAS-*f*-CNTs	$5.2*10^5$

Concerning the nanocomposites, bare and COOH-functionalized CNTs slightly increase the UHMWPE oxidation induction time without substantially altering the slope of the CI and HI curves, i.e. the rate of formation of the oxidized species. The UHMWPE/HAS-*f*-CNTs nanocomposite exhibits the best photo-oxidation resistance, in terms of both delayed induction time and decreased rate of oxygen containing species formation. It is important to stress that such a result has been achieved at an overall content of linked HAS much lower than what added as free additive in the sample UHMWPE/UV-3853.

Non-volatile UV-3853 stabilizer is efficient in the protection of the polymeric matrix against photo-oxidation, but the stabilizing actions achieved in our sample filled with HAS-*f*-CNTs is much higher than what one would expect considering the effect of adding UV-3853 and CNTs separately. We argue that the protective activity of HAS-*f*-CNTs can be ascribed to three main mechanisms: (i) inherent protection action of CNTs exacerbated by the presence of covalently linked HAS molecules, (ii) reduced migration/segregation of HAS, (iii) stabilizing action of HAS explicated at the interfacial region.

CNTs act as inner filters similarly to carbon black, thus stabilizing polymeric matrices against photo-oxidation [30,31]. Furthermore CNTs, when exposed simultaneously to UV light and oxygen, may experience photoinduced oxidation, with formation of locally electron-deficient and electron-rich regions on the nanotubes surface, whose make possible the adsorption of oxygen molecules on the nanotubes [32]. Being strongly bonded on the walls of carbon nanotubes, the oxygen molecules cannot contribute to the oxidation of the polymer matrix [33].

Due to the presence of acceptor-like localized states, CNTs are also able to exert a radical scavenging activity. This inherent ability can be enhanced generating structural defects on the CNT outer surface, for example, by means of chemical functionalization [18,19]. As assessed by Raman spectroscopy, the structural defects concentration is in the following order: HAS-*f*-CNTs > CNTs-COOH > CNTs, which is in agreement with the stabilizing activity against photo-oxidation shown in Fig. 9. We can hence conclude that the covalent linkage of HAS molecules increases the amount of defects onto CNTs surface, probably improving the radical scav-enging activity of CNTs. This hypothesis has been recently docu-mented both experimentally [15–17] and theoretically [34].

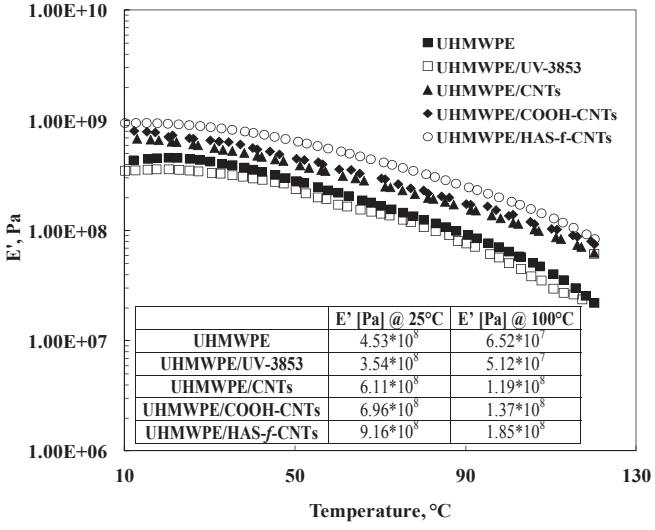

Fig. 8. Elastic modulus E′ as a function of temperature for all investigated systems.

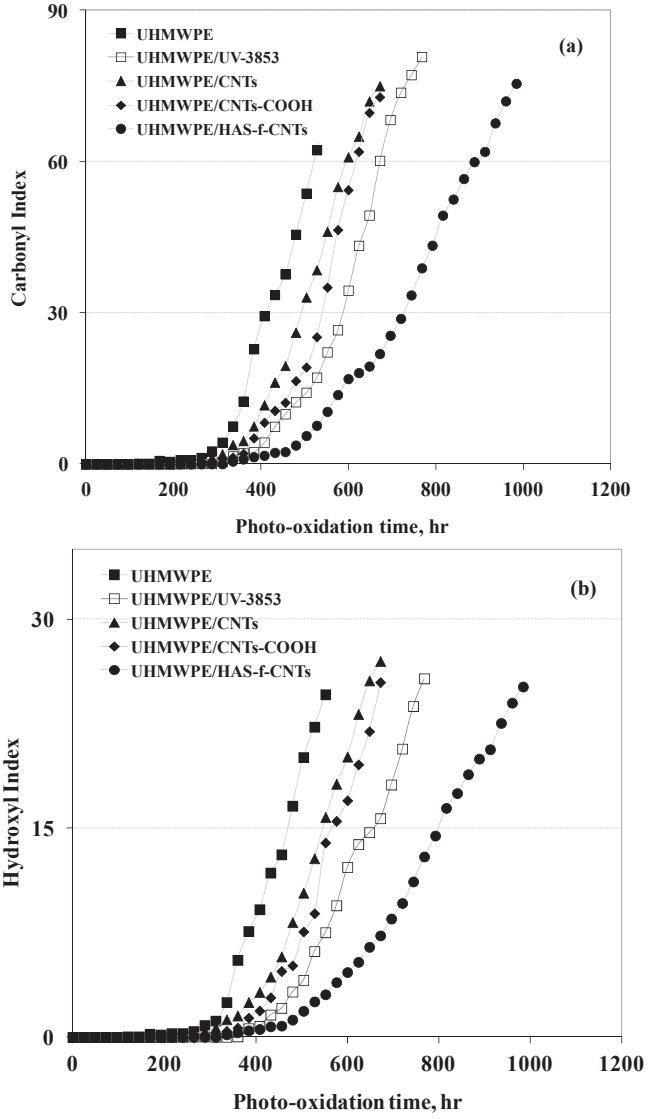

Fig. 9. Carbonyl (a) and hydroxyl (b) indices as a function of the photo-oxidation time for all investigated systems.

Table 2
Values of the photo-oxidation induction time.

	t_i @ CI = 5 [h]	t_i @ HI = 2 [h]
UHMWPE	310	325
UHMWPE/UV-3853	405	450
UHMWPE/CNTs	362	375
UHMWPE/CNTs-COOH	378	410
UHMWPE/HAS-*f*-CNTs	495	508

Another beneficial effect of using HAS-*f*-CNTs may come from the hindered migration/segregation of the HAS molecules. The covalently linked stabilizing molecules can exert their protective action for a longer time compared to their free counterpart. Moreover, being immobilized at the polymer−nanoparticle interface, the HAS exerts their stabilizing action in a critical region for the photo degradation processes. In fact, the photo-oxidation rate of polymer-based micro- and nanocomposites is known to increase with increasing interface area between matrix and fillers [35,36]. The reason is that the formation of radicals occurs more rapidly at the polymer−particle interface, where there is a greater availability of environmental oxygen.

4. Conclusions

CNTs bearing covalently linked HAS molecules have been prepared and characterized through spectroscopic, spectrometric and thermo-gravimetric analyses. The covalent nature of the link between nanotubes and stabilizer has been ascertained. It was found that the chemical functionalization generates structural defects on the CNT surface. The functionalized CNTs have been compounded with UHMWPE to prepare composite films by hot-compaction. Morphological analyses have revealed a segregated morphology, characterized by electrically conductive CNT-rich channels that surround the polymer particles. Rheological, electrical and DMA analyses have demonstrated that the HAS-*f*-CNTs are better distributed than bare CNTs. More importantly, it was found that the films containing HAS-*f*-CNTs exhibit enhanced photo-oxidative resistance compared to films in which HAS and CNTs are added separately. A synergic effect of CNTs and HAS molecules has been conjectured. In particular, the chemical functionalization is believed to induce the formation of sidewall defects that act as acceptor-like localised states, thus providing an additional free-radical scavenging activity to the CNTs. In addition, the covalent grafting of HAS on the CNT outer surface maximizes the exposure of the HAS molecules towards the polymer and hinders their migration/segregation, allowing for a better exploitation of their inherent UV-stabilizing action.

Acknowledgements

This work has been financially supported by Ministry of University and Research in Italy (MIUR), FIRB2010 − Futuro in Ricerca, Project title: “GREENER − Towards multifunctional, efficient, safe and stable “green” bio-plastics based nanocomposites of technological interest via the immobilization of functionalized nanoparticles and stabilizing molecules” (cod: RBFR10DCS7).

References

[1] Noorden RV. The trials of new carbon. Nature 2011;469(7328):14−6.
[2] Xu JZ, Zhong GJ, Hsiao BS, Fu O, Li ZM. Low-dimensional carbonaceous nanofiller induced polymer crystallization. Prog Polym Sci 2013;39(3): 555−93.
[3] Arrigo R, Dintcheva NT, Morici E, La Mantia FP. Performances and morphology of polyamide/carbonaceous structures based fibers. AIP Proc 2014;1599: 330−3.
[4] Spitalsky Z, Tasis D, Papagelis K, Galiotis C. Carbon nanotube−polymer composites: chemistry, processing, mechanical and electrical properties. Prog Polym Sci 2010;35(3):357−401.
[5] Dintcheva NT, Arrigo R, Morreale M, La Mantia FP, Matassa R, Caponetti E. Effect of elongational flow on morphology and properties of polymer/CNTs nanocomposite fibers. Polym Adv Tech 2011;22(12):1612−9.
[6] (a) Dintcheva NT, Arrigo R, Nasillo G, Caponetti E, La Mantia FP. On the role of extensional flow in morphology and properties modifications in MW-CNTs polyamide-based fibres. Macromol Mater Eng 2011;296(7): 645−57.
(b) Yang M, Gao Y, Li H, Adronov A. Functionalization of multiwalled carbon nanotubes with polyamide 6 by anionic ring-opening polymerization. Carbon 2007;45(12):2327−33.
[7] (a) Dintcheva NT, Arrigo R, Nasillo G, Caponetti E, La Mantia FP. Effect of the nanotube aspect ratio and surface functionalization on the morphology and properties of multiwalled carbon nanotube polyamide-based fibers. J Appl Polym Sci 2013;129:2479−89.
(b) Nativ-Roth E, Shvartzman-Cohen R, Bounioux C, Florent M, Zhang D, Szleifer I, et al. Physical adsorption of block copolymers to SWNT and MWNT: a nonwraping mechanism. Macromolecules 2007;40(10):3676−85.
[8] Mawhinney DB, Naumenko V, Kuznetsova A, Yates JT, Liu J, Smalley RE. Surface defect site density on single walled carbon nanotubes by titration. Chem Phys Lett 2000;324(1−3):213−6.
[9] Campidelli S, Ballesteros B, Filoramo A, Dıaz DD, Torre G, Torres T, et al. Facile decoration of functionalized single-wall carbon nanotubes with phthalocyanines via click chemistry. J Am Chem Soc 2008;130(34):11503−9.
[10] Roy N, Sengupta R, Bhowmick AK. Modifications of carbon for polymer composites and nanocomposites. Prog Polym Sci 2012;37(6):781−819.
[11] Sahoo NG, Rana S, Cho JW, Li L, Chan SH. Polymer nanocomposites based on functionalized carbon nanotubes. Prog Polym Sci 2010;35(7):837−67.
[12] Karousis N, Tagmatarchis N. Current progress on the chemical modification of carbon nanotubes. Chem Rev 2010;110(9):5366−97.
[13] Wang J, Yuan R, Chai Y, Cao S, Guan S, Fu P, et al. A novel immunosensor based on gold nanoparticles and poly-(2,6-pyridinediamine)/multiwall carbon nanotubes composite for immunoassay of human chorionic gonadotrophin. Biochem Eng J 2010;51(3):95−101.
[14] Chen RJ, Zhang Y, Wang D, Dai H. Noncovalent sidewall functionalization of single-walled carbon nanotubes for protein immobilization. J Am Chem Soc 2001;123(16):3838−9.
[15] Dintcheva NT, Arrigo R, Gambarotti C, Carroccio S, Filippone G, Cicogna F, et al. a-Tocopherol-induced radical scavenging activity in carbon nanotubes for thermo-oxidation resistant ultra-high molecular weight polyethylene-based nanocomposites. Carbon 2014;74:14−21.
[16] Dintcheva NT, Arrigo R, Gambarotti C, Guenzi M, Carroccio S, Cicogna F, et al. Immobilization of natural anti-oxidants on carbon nanotubes and aging behavior of ultra-high molecular weight polyethylene-based nanocomposites. AIP Conf Proc 2014;1599:102−5.
[17] Arrigo R, Dintcheva NT, Guenzi M, Gambarotti C, Filippone G, Coiai S, et al. Thermo-oxidative resistant nanocomposites containing novel hybrid-nanoparticles based on natural polyphenol and carbon nanotubes. Polym Degrad Stab 2015;115:129−37.
[18] Watts PCP, Fearon PK, Hsu WK, Billingham NC, Kroto HW, Walton DRM. Carbon nanotubes as polymer antioxidants. J Mater Chem 2003;13: 491−5.
[19] Shi X, Jiang B, Wang J, Yang Y. Influence of wall number and surface functionalization of carbon nanotubes on their antioxidant behaviour in high density polyethylene. Carbon 2012;50(3):1005−13.
[20] Conyers JL, Lucente-Schultz RM, Moore VC, Leonard AD, Price BK, Kosynkin DV, et al. Antioxidant single-walled carbon nanotubes. J Am Chem Soc 2009;131(11):3934−41.
[21] Lonkar SP, Kushwaha OS, Leuteritz A, Heinrichac G, Singh RP. Self photostabilizing UV-durable MWCNT/polymer nanocomposites. RSC Adv 2012;2(32):12255−62.
[22] Gensler R, Plummer CJG, Kausch HH, Kramer E, Pauquet JR, Zweifel H. Thermo-oxidative degradation of isotactic polypropylene at high temperatures: phenolic antioxidants versus HAS. Polym Derg Stab 2000;67: 195−208.
[23] Gijsman P, Smelt HJ, Schumann D. Hindered amine light stabilizers: an alternative for radiation cross-linked UHMWPE implants. Biomaterials 2010;31:6685−91.
[24] Puértolas JA, Kurtz SM. Evaluation of carbon nanotubes and graphene as reinforcements for UHMWPE-based composites in arthroplastic applications. A Rev J Mech Behav Biomed 2014;39:129−45.
[25] Chukov DI, Stepashkin AA, Maksimkin AV, Tcherdyntsev VV, Kaloshkin SD, Kuskov KV, et al. Investigation of structure, mechanical and tribological properties of short carbon fiber reinforced UHMWPE-matrix composites. Compos Part B 2015;76:79−88.
[26] Suner S, Joffe R, Tipper JL, Emami N. Ultra high molecular weight polyethylene/graphene oxide nanocomposites: thermal, mechanical and wettability characterisation. Compos Part B 2015;78:185−91.
[27] Silverstein RM, Webster FX, Kiemle DJ. Spectrometric identification of organic compounds. 7th ed. John Wiley and Sons, Inc; 2005.
[28] Qian WZ, Liu T, Wei F, Yuan HY. Quantitative Raman characterization of the mixed samples of the single and multi-walled carbon nanotubes. Carbon 2003;41:1851−4.
[29] Holzinger M, Abraham J, Whelan P, Graupner R, Ley L, Hennrich F, et al. Functionalization of single-walled carbon nanotubes with (R-)oxycarbonyl nitrenes. J Am Chem Soc 2003;125(28):8566−80.
[30] Morlat-Therias S, Fanton E, Gardette JL, Peeterbroeck S, Alexandre M, Dubois P. Polymer/carbon nanotube nanocomposites: influence of carbon nanotubes on EVA photodegradation. Polym Degr Stab 2007;92(10): 1873−82.
[31] Dintcheva NT, La Mantia FP, Malatesta V. Photo-oxidation behaviour of polyethylene/multi-wall carbon nanotube composite films. Polym Degrad Stab 2009;94(2):162−70.

[32] Savage T, Bhattacharya S, Sadanadan B, Gaillard J, Tritt TM, Sun YP, et al. Photoinduced oxidation of carbon nanotubes. J Phys Condens Matter 2003;15: 5915–21.
[33] Guadagno L, Naddeo C, Raimondo M, Gorrasi G, Vittoria V. Effect of carbon nanotubes on the photo-oxidative durability of syndiotactic polypropylene. Polym Degrad Stab 2010;95(9):1614–26.
[34] Galano A. Carbon nanotubes as free-radical scavengers. J Phys Chem C 2008;112(24):8922–7.
[35] Morreale M, Dintcheva NT, La Mantia FP. The role of filler type in the photo-oxidation behaviour of micro- and nano-filled polypropylene. Polym Int 2011;60:1107–16.
[36] Morreale M, Dintcheva NT, La Mantia FP. Accelerated weathering of PP based nanocomposites: effect of the coupling agent. Ex-Press Polym Lett 2013;7: 703–15.